Journal of Magnetic Resonance **144,** 243–254 (2000)
doi:10.1006/jmre.2000.2041, available online at http://www.idealibrary.com on IDEAL®

High-Resolution Diffusion Imaging Using a Radial Turbo-Spin-Echo Sequence: Implementation, Eddy Current Compensation, and Self-Navigation

Markus H. J. Seifert,* Peter M. Jakob,* Vladimir Jellus,† Axel Haase,* and Claudia Hillenbrand*,[1]

*Lehrstuhl für Experimentelle Physik V, Physikalisches Institut der Universität Würzburg, Germany; and †Institute of Measurement Science, Bratislava, Slovakia

Received September 1, 1999; revised January 13, 2000

This work describes a segmented radial turbo-spin-echo technique (DW-rTSE) for high-resolution multislice diffusion-weighted imaging and quantitative ADC mapping. Diffusion-weighted images with an in-plane resolution of 700 μm and almost free of bulk motion can be obtained *in vivo* without cardiac gating. However, eddy currents and pulsatile brain motion cause severe artifacts when strong diffusion weighting is applied. This work explains in detail the artifacts in projection reconstruction (PR) imaging arising from eddy currents and describes an effective eddy current compensation based on the adjustment of gradient timing. Application of the diffusion gradients in all three orthogonal directions is possible without degradation of the images due to eddy current artifacts, allowing studies of the diffusional anisotropy. Finally, a self-navigation approach is proposed to reduce residual nonrigid body motion artifacts. Five healthy volunteers were examined to show the feasibility of this method. © 2000 Academic Press

Key Words: **radial; diffusion imaging; turbo-spin-echo; high resolution; eddy current.**

INTRODUCTION

Spatial mapping of diffusion coefficients provides an additional contrast mechanism in MRI which can be used to obtain important physiological information on water mobility, compartmentation, and diffusional anisotropy (*1–3*). Animal and human studies have suggested that diffusion-weighted imaging (DWI) is a sensitive indicator for early detection of ischemic injury, since areas of acute stroke show a drastically lowered diffusion coefficient (*4–7*). The application of DWI to an animal model of multiple sclerosis has been discussed (*8*). However, methodological limitations exist for the widespread application of DWI in humans. Conventional methods of acquiring diffusion-weighted images involve the use of Stejskal–Tanner diffusion-sensitized gradients (*9, 10*) in conjunction with spin-echo 2D Fourier transform acquisition. One of the great obstacles in clinical DWI is that the image quality and quantitative diffusion measurements are severely degraded by even small macroscopic motions of the head and brain. The reason for this high motion sensitivity is the large pulsed gradients required for the Stejskal–Tanner diffusion preparation. Pulsatile brain motion can be controlled by cardiac gating, but rigid body motion still remains a problem. Several strategies have been developed in the past to overcome the motion sensitivity problem:

(i) Single shot DWI techniques, despite their lower spatial resolution, are currently the method of choice, since they "freeze out" the effects of macroscopic motion and allow a high scan efficiency. Echo planar diffusion imaging (*11, 12*) has been used successfully for measuring diffusion of water in the brain of volunteers and patients (*13*) and is generally now regarded as the method of reference. However, echo-planar imaging (EPI) is very sensitive to magnetic susceptibility artifacts resulting in image distortions and off-resonance artifacts, which require efficient shim procedures and fat-suppression schemes. The resolution achievable with EPI is limited due to T_2^* decay during the echo train. In addition, special gradient hardware is necessary for the EPI technique. Therefore, less demanding single-shot DWI approaches for clinical scanners including high-speed STEAM (*14*), turbo-FLASH (*15*), and GRASE (*16*) have been developed. These rapid imaging techniques are generally much less motion sensitive, but often compromise spatial resolution and signal-to-noise ratio (SNR). Fast diffusion imaging based on a steady-state-free precession scheme has also been proposed (*17–19*).

(ii) Another approach to reduce rigid body motion artifacts in multi-shot DWI is based on navigator echoes (*20–22*). The navigator echoes provide a measure of the motion-induced view-to-view phase variations utilizing an additional non-phase-encoded echo acquired before the imaging echo. The image data can then be corrected retrospectively for linear velocity and acceleration of the head. However, the navigator approach appears to be of limited value when complex motion, e.g. brain pulsation, is involved.

(iii) Another approach to reduce motion artifacts in DWI is

[1] To whom correspondence should be addressed. E-mail: hillenbrand@physik.uni-wuerzburg.de.

1090-7807/00 $35.00

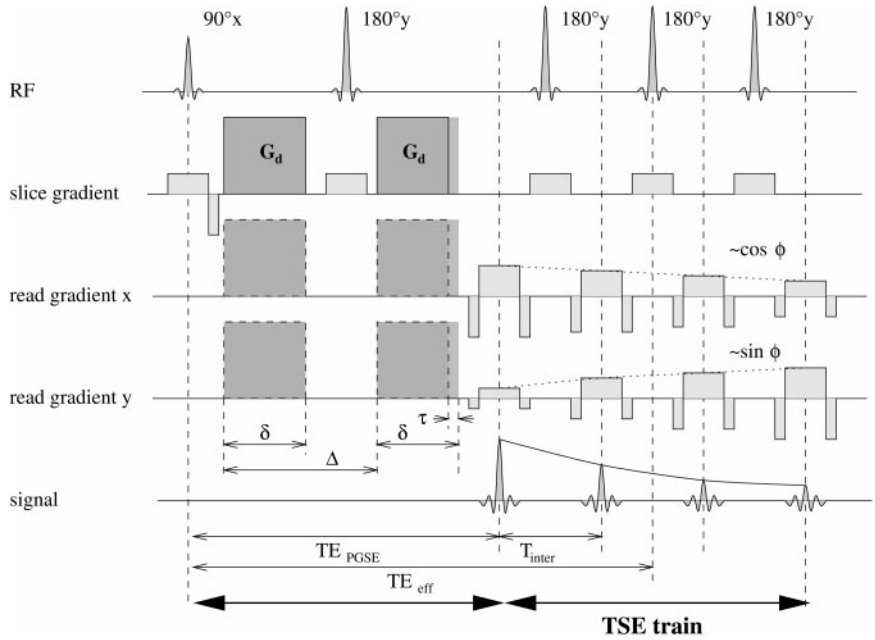

FIG. 1. Schematic presentation of the diffusion-weighted radial turbo-spin-echo sequence: The DW-rTSE sequence consists of a pulsed gradient spin-echo (PGSE) preparation phase and a radial turbo-spin-echo (TSE) readout. All RF pulses are slice selective filtered sinc-pulses. The effective echo time TE_{eff} was given by $TE_{eff} = TE + (N/2 - \frac{1}{2}) \cdot T_{inter}$ with N being the number of echoes per echo train. In the experiments done for this study four projections were acquired after one excitation.

projection reconstruction (PR) imaging. In PR imaging radial lines in Fourier space are acquired instead of rectilinear lines as in 2D Fourier transform (2D FT) imaging. Therefore these sequences are called radial sequences. PR imaging in general shows a reduced sensitivity to motion (*23*) and flow artifacts (*24*) in combination with magnitude reconstruction. In addition, it offers a slight gain in signal-to-noise ratio and is less susceptible to phase errors when compared to 2D FT imaging (*25*). Radial sequences have been used for DWI (*28, 29, 31*), but eddy current problems have been reported when applying the diffusion gradients in the same orientation as the read gradients (*30*). Some groups (*24, 33*) used rotating diffusion gradients to eliminate remaining motion artifacts. This has the disadvantage that the diffusion anisotropy cannot be measured.

Since measurement times in standard radial imaging are comparable with conventional spin-echo imaging, the acquisition of several echoes after one excitation has been proposed to increase the speed of PR imaging (*26, 27*). Recently, it has been shown that this radial turbo-spin-echo approach can also be combined with diffusion contrast in order to obtain high-resolution diffusion weighted images with increased imaging speed and reduced sensitivity to motion (*31, 32*).

In this study we present a radial multislice turbo-spin-echo DWI sequence which includes eddy current compensation and self-navigation to reduce artifacts due to eddy currents and pulsatile brain motion. This sequence provides quantitative high-resolution diffusion imaging and diffusional anisotropy measurements in all areas of the human brain, even if strong diffusion weighting is applied. In this contribution, the main components for a successful implementation of such a sequence are summarized: First there will be a brief description of the sequence design and the image reconstruction. Then artifacts resulting from eddy currents in radial DWI will be explained, and a method for eliminating these artifacts will be suggested. A self-navigation method for reducing nonrigid body motion artifacts will be proposed. After the description of the experimental setup, typical results obtained from diffusion imaging experiments performed in phantoms and in the human brain of healthy volunteers will be presented.

METHODS AND EXPERIMENTAL

Implementation and Image Reconstruction

The pulse sequence (Fig. 1) for diffusion-weighted radial turbo-spin-echo (DW-rTSE) imaging consists of two parts: (i) a standard pulsed gradient spin-echo (PGSE) preexperiment including eddy current compensation and (ii) a radial turbo-spin-echo readout train. The slice selective PGSE experiment creates a transverse magnetization M at the echo time TE weighted with T_2 and the diffusion coefficient D (*9*)

$$\frac{M(TE)}{M(0)} = e^{-TE/T_2} \cdot e^{-bD}, \qquad [1]$$

where b is the well-known "b value," which is a measure for

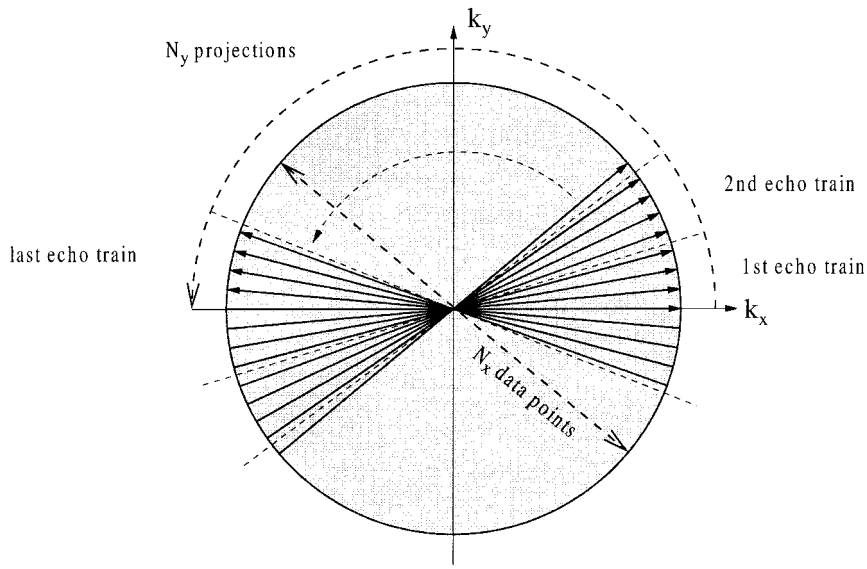

FIG. 2. Coverage of the *k* space. The direction of the radial lines is stepped sequentially from 0° to 180° with each echo. For a final image matrix size of $N_x \times N_y$ pixels N_x data points in read direction and N_y projections were acquired.

the diffusion-weighting. The *b* value for a balanced pair of gradients of strength G_d, duration δ, and separation Δ is given by (*9*)

$$b = \gamma^2 G_d^2 \delta^2 \left(\Delta - \frac{\delta}{3} \right). \qquad [2]$$

This attenuated echo formed by the PGSE experiment is the first echo of the turbo-spin-echo readout train which is refocused multiple times by 180° RF pulses to acquire more than one projection after a single preparation. Each echo is encoded with the readout gradient $\vec{G}_r = G_r \cdot (\vec{e}_x \cos\phi + \vec{e}_y \sin\phi)$ applied under different angles ϕ in the image plane. For a resulting image with a rectangular matrix of $N_x \times N_y$ pixels, N_y projections under increasing in-plane angles ϕ with N_x data points in the radial direction were acquired. The angle ϕ was incremented from 0 to 180° in steps of $\Delta\phi = (180°/(N_y + 1))$. In the actual implementation a sequential sampling of *k* space was performed (Fig. 2). Each echo train consisting of *N* echoes covered a segment of the *k* space with an angle $\alpha = N \cdot \Delta\phi$. However, interleaved sampling as noted in (*31*) is also possible.

Since imperfect 180° pulses may populate higher order phase states (*36, 37*), the rephasing back to the center of *k* space guarantees a zero phase accumulation $\int G(t)dt = 0$ due to the read gradients between succeeding RF pulses. This ensures that the echoes from different echo families will experience identical spatial encoding.

In the following, the image reconstruction of radial data using a filtered backprojection algorithm is shortly described. The filtered backprojection from the acquired signal $S(k, \phi)$ is split into three major parts:

1. The magnitude of the Fourier transform of the signals is calculated giving the raw projections

$$p(\phi, R) = (2\pi)^{-1} \left| \int_{-\infty}^{+\infty} S(k, \phi) e^{-ikR} dk \right|$$

with $R := (x \cos\phi + y \sin\phi)$ and the k-space vector $\vec{k} = \gamma \vec{G}_r t$. These raw projections are summarized in the sinogram.

2. The raw projections $p(\phi, R)$ are filtered with a convolution filter giving the filtered projections p^* along the read gradient direction.

3. The projections are backprojected to form an image $\rho(x, y) = \int_0^{\pi} p^*(\phi, R) d\phi$ on a Cartesian grid.

The choice of the convolution filter applied to the raw projections is essential for the final image quality. For all images in this work, the filter published in (*38*) produced a good image quality with reduced streaking artifacts and background noise.

One problem particular to DWI is that the presence of patient motion, eddy currents, and flow disturb the phase of the echoes. Typically these phase disturbances are not constant during the experiment. By using the backprojection algorithm in the magnitude mode, the phase inconsistencies predominantly affect the amplitude of the different projections. This amplitude modulation is smeared out over the whole image due to the inherent averaging effect in PR (*27*). Therefore, small random phase errors lead to artifacts of negligible amplitude in the resulting image, making PR imaging in combination with magnitude reconstruction much more insensitive to phase effects than conventional 2D-FT imaging. However, there are

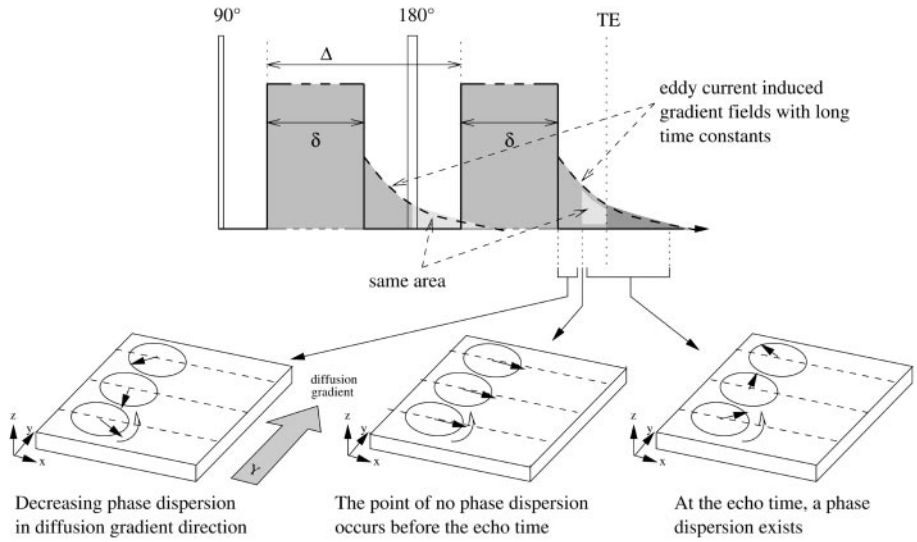

FIG. 3. Eddy current and phase dispersion effects in PGSE experiments. Eddy currents produce long-term gradient fields, which still exist after the 180° RF pulse of the PGSE experiment. This leads to a nonzero phase dispersion at the echo time TE in the direction of the diffusion gradient.

imaging situations, where significant effects of phase induced amplitude errors are apparent in PR-DWI. This is demonstrated in the following sections.

Eddy Current Effects and Their Compensation

The eddy currents induced by switching of large diffusion gradients are a great obstacle in DWI. This leads to additional magnetic field gradients and an unwanted phase dispersion after the preparation. Despite improvements in gradient hardware, such as actively shielded gradients, these problems still occur. A general analysis of eddy current behavior has been performed by Ahn and Cho (*39*). Several approaches to avoid these problems have been proposed for diffusion weighted EPI (*40*).

In the following, we propose a simple but robust eddy current compensation for radial DW imaging based on the adjustment of the gradient timing. This method is based on the following considerations: Ramping down large gradients induces eddy currents, which produce a gradient field of the same polarity as the original gradient (*39*). Switching off of the first diffusion gradient of the PGSE preparation produces an eddy current gradient field which may still exist after the 180° RF pulse of the PGSE preparation, depending on the time constant of the eddy currents (Fig. 3). This gradient field increases the gradient integral in the second half of the PGSE experiment. Therefore, the integrals over the gradient will be different in the first and the second half of the PGSE experiment, leading to a nonzero phase dispersion

$$\varphi(TE) = \gamma\left(\int_0^{TE/2} G_d(t)dt - \int_{TE/2}^{TE} G_d(t)dt\right)\Delta s \neq 0 \quad [3]$$

of the transversal magnetization at the echo time, TE, where Δs represents the spatial distance from the center of the magnet in the direction of the diffusion gradients.

This phase dispersion has different effects on each projection depending on the angle between diffusion and readout gradient. If the diffusion gradient is applied in the image plane, severe eddy current artifacts can occur. In PR imaging, the measured signal is proportional to the sum of the transverse magnetization $M_{xy}(x, y)$ along a line perpendicular to the readout gradient G_r (*25*). In case of a nonconstant phase $\varphi(x, y) \neq const.$ in the image plane, negative and positive interference will take place depending on the phases of the signal components. If diffusion and readout gradient are parallel, no negative interference will take place, since only signal components of equal phase will be summed up (see Fig. 4A). However, negative interference will occur in the case of nonparallel diffusion and readout gradients, leading to severe image artifacts (see Fig. 4B). The subsequent echoes of the turbo-spin-echo readout will also be affected since the eddy current effects lead to a nonconstant phase accumulation during the echo train and the CPMG condition will no longer be satisfied. In contrast, if the diffusion gradient is applied perpendicular to the image plane, a phase dispersion in slice direction occurs. Since the slice thickness is usually small compared to the image field of view, this phase dispersion is also small and leads to a slight signal loss. Due to constant phases in all read directions (see Fig. 4C) no severe image artifacts will arise. Therefore, diffusion-weighting in slice direction is less critical in terms of image artifacts.

Rotating the diffusion gradient in-plane to be always parallel to the read-out gradient may avoid eddy current induced image artifacts in the case of in-plane diffusion-weighting. However,

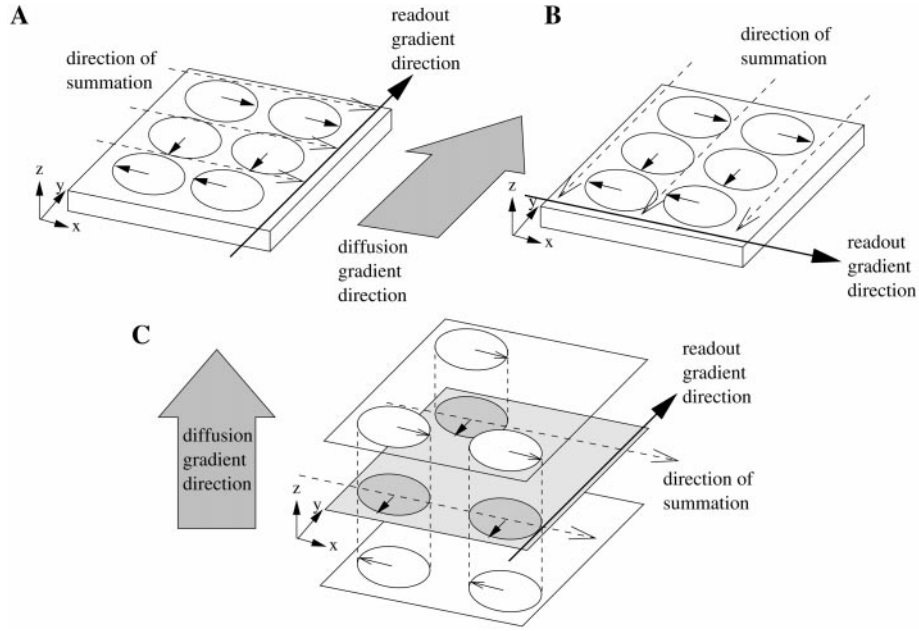

FIG. 4. Effects of a phase dispersion in PR imaging. If the diffusion gradient is (A) parallel to the readout gradient, no image artifacts will be produced by the phase dispersion because signal components of equal phase will be summed up to form the signal. In the case of (B) nonparallel or even perpendicular gradients different signal phases will be summed up and interference will disturb the resulting signal leading to severe image artifacts. If the diffusion gradient is applied (C) through-plane only a small negative interference will occur due to the small phase dispersion through the imaging plane. This phase dispersion is small because the slice thickness is much smaller than the field of view with the phase dispersion per unit length being equal to those cases shown in (A) and (B). But no negative interference will occur during readout in the planes perpendicular to the phase dispersion, since all signal components have the same phase in these planes. Therefore, only a small uniform signal loss will be produced.

this approach suffers from the major disadvantage that measurements of diffusional anisotropy are not possible. Therefore, another strategy was chosen to compensate for the effects of the eddy current induced phase dispersion.

The phase dispersion can be avoided by introducing a trim time τ to shorten the second diffusion gradient to a duration of $\delta' = \delta - \tau$. This compensates the additional gradients caused by the eddy currents so that the diffusion gradients now fulfill the condition $\int_0^{TE/2} G_d dt = \int_{TE/2}^{TE} G_d dt$ for zero phase dispersion at the echo time *TE* of the first echo. This eliminates the major, short-time-constant eddy current induced contribution to phase accumulation during the echo train. Eddy currents with long-time constants may still be present during later echoes, but in our experience they are usually significantly lower in amplitude and therefore do not cause major artifacts (see Fig. 5).

The experimentally determined trim time τ is very short on our system ($\tau = 10$–20 μs depending on the gradient used as diffusion gradient) compared with the typical diffusion gradient duration ($\delta \sim 25$ ms) but it eliminates effectively eddy current induced image artifacts as demonstrated in Fig. 5. The shortness of the trim time indicates that a small difference in the integral over the gradients in both halves of the PGSE experiment causes a significant phase dispersion at the echo time *TE* (according to Eq. [3]) this dispersion is equal to $\varphi/\Delta y \approx 40°$/cm for our system using a diffusion gradient of 29 mT/m and 5 ms separation from switching off the second diffusion gradient to the first echo). The trim time must be determined once for the actual system configuration and for each gradient used. The determination of the trim time is done by varying the trim time until maximum signal is achieved in all projections. This approach has the advantage compared with trimming the gradient strength, that the trim time, once determined, is independent of the actual gradient strength G_d and duration δ used, as long as eddy current effects are directly proportional to the gradient strength G_d. Otherwise an individual trim time must be determined for each gradient strength G_d.

Motion Sensitivity and Self-Navigation

PR imaging has been proven to be relatively insensitive to rigid body motion artifacts which only cause a slight blurring of the images (*28*). However, brain pulsation artifacts may still affect image quality in PR imaging. Brain motion in the presence of magnetic field gradients leads to a velocity dependent phase, $\varphi = \gamma G_d v \Delta\delta$, for a given velocity v. Thus, in the presence of significant in-plane brain motion during the PGSE preparation, projections with nonparallel diffusion and readout gradients can be severely degraded by phase dispersions similar to those caused by eddy currents. Through-plane motion-induced phase errors also reduce the signal amplitude as a function of the applied *b* value. This is particularly a problem

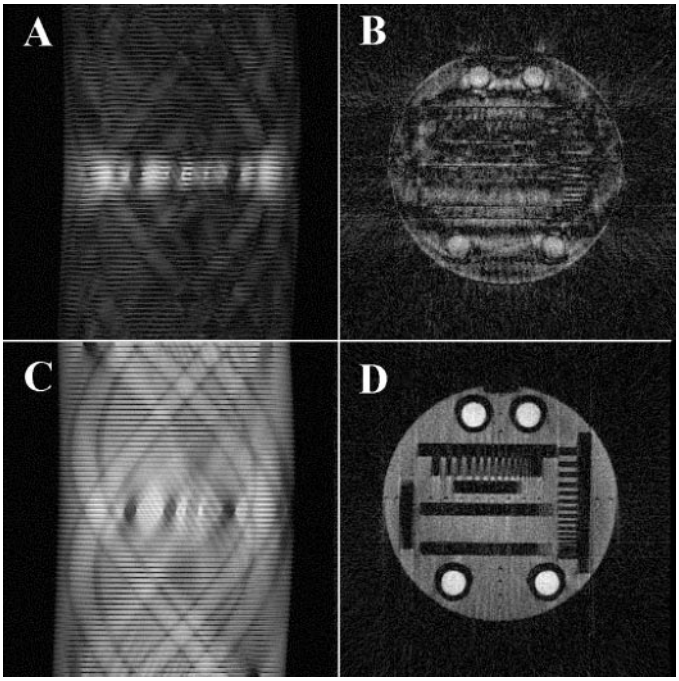

FIG. 5. Eddy current compensation: (A) shows a sinogram without eddy current compensation. Most projections are affected by eddy current effects except those where the diffusion gradient is parallel to the readout gradient (the bright projections in the middle); (B) is the corresponding image reconstructed from the projections shown in (A). The image suffers from severe artifacts; (C) shows the sinogram acquired with effective eddy current compensation; (D) is the corresponding image from the projections in (C). All data were acquired with the same b value ($b = 806$ s/mm^2) and the diffusion gradient in top/bottom direction.

in inferior axial slices of the human brain when the diffusion gradient is applied in the head/foot direction. In general, the result of motion is that the measured ADC will tend to be overestimated in an uncorrected *in vivo* scan.

ECG-triggering can be used to avoid this motion-induced phase dispersion. However, this significantly increases the total acquisition time in multislice experiments since ideally each slice must be acquired in a phase of negligible brain motion. If no ECG-triggering is used, only a certain number of projections will be disturbed. In our experience, less than one third of all projections acquired are degraded (e.g., see Fig. 7D). With this number of degraded projections, backprojection still produces usable images, where a significant signal attenuation only occurs in the regions of strong brain pulsation.

To obtain images with reduced pulsation artifacts, a self-navigator approach was developed. This technique uses acquired projections as their own motion navigator. In case of no pulsatile motion, i.e., negligible phase dispersion during the readout period, all spins in the image plane add up coherently to form the final signal. Each spin will contribute to different frequency components of the signal from projection to projection, depending on the direction of the rotating readout gradient. However, the sum over all signal components remains constant for each projection as long as imaging parameters and spin density are unchanged. Therefore, the energy of the projections, which is often referred to as the projection integral, remains constant $E = \int_{-\infty}^{+\infty} p(\phi, R)dR = const.$ for all ϕ (*47*). Since motion in a field gradient causes a phase dispersion and therefore a reduced signal amplitude, a reduced projection energy is produced. This can be detected automatically by an algorithm which compares the energy of each projection with a predefined threshold, e.g., defined by the mean energy of all projections. If the energy is below this threshold, the projection is judged to be degraded and will be acquired again. In this study, this self-navigation principle was implemented as an offline procedure, where approximately 30% of the acquired projections were discarded and reacquired in an independent scan.

Experimental

All data were acquired using a 2.0 Tesla whole body MRI system (Tomikon S200, Bruker Medical Systems, Ettlingen, Germany) with a maximum gradient strength of 31 mT/m and a minimum gradient rise time of 600 μs. In our experiments the echo train length was limited to four echoes to minimize the effect of T_2 relaxation on the image contrast. Hence the contrast behavior was almost comparable to standard spin-echo DWI. A typical multislice (5 slices) experiment was performed with a repetition time of $TR = 1$ s. Diffusion gradients with $\delta = 25$ ms and a maximum strength of $G_d = 25$ mT/m were applied. In all experiments, the proposed eddy current compensation was applied. Trim times were $\tau_x = 10$ μs, $\tau_y = 11$ μs, and $\tau_z = 19$ μs. Slice selective filtered and truncated sinc-pulses with a duration of 2 ms were used as refocusing pulses. The inter echo time T_{inter} was approximately 10 ms depending on the matrix size and the imaging bandwidth. Field of view was 36 cm in combination with a 512×512 matrix. The imaging gradients consisted of a 500 μs dephasing section, followed by the readout section with the echo in the center of the acquisition window and a 500 μs rephasing section. For all studies no fat suppression was used. For quantitative imaging, a series of images were acquired keeping N, T_{inter}, and TE constant, but with variable G_d. From this series of images, the apparent diffusion coefficient (ADC) was calculated using a pixel-by-pixel nonlinear fit algorithm.

The DW-rTSE sequence was first evaluated in a stationary, spherical phantom containing doped water. The experiments were performed at room temperature. The diffusion coefficient was measured in all three orthogonal directions x, y, and z with 2 b values of 1.7 and 692 s/mm^2. *In vivo* experiments were performed in five healthy volunteers in order to demonstrate the feasibility and stability of this sequence. In addition, ECG-gated images were acquired in order to obtain reference images free of pulsation artifacts. These reference images were used to compare (i) gated versus nongated acquisitions in slices with no significant pulsatile motion and (ii) self-navigated versus

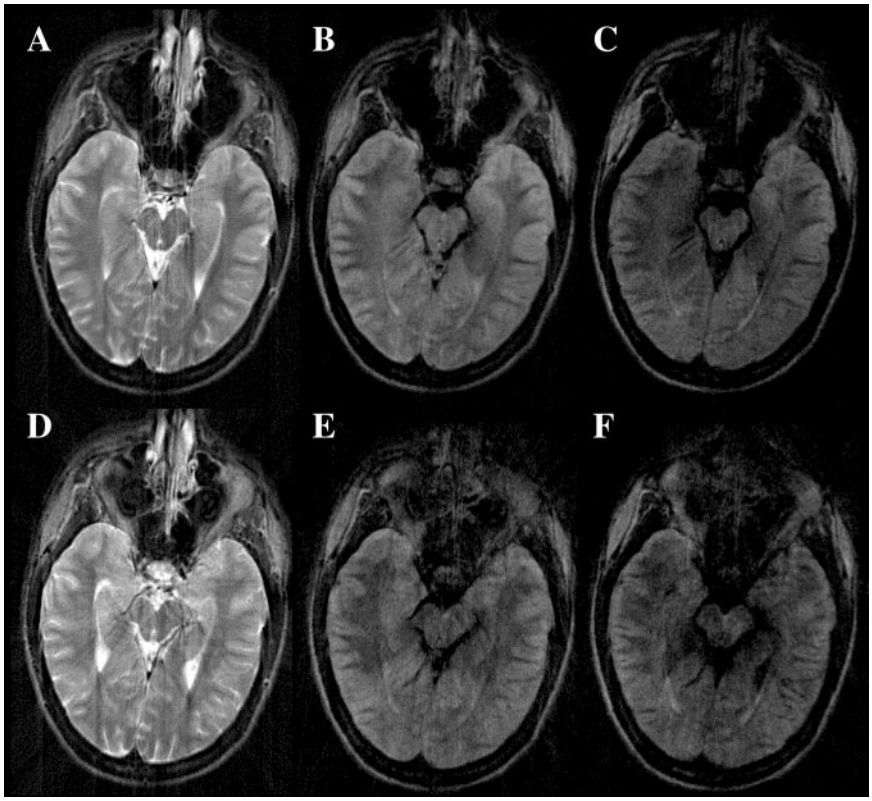

FIG. 6. Effect of ECG-gating: Diffusion weighted images acquired with ECG-gating (A–C) and without ECG-gating (D–F) are shown (FOV = 36.0 cm, 512 × 512 matrix, $TR = 1$ s, $TE_{PGSE} = 60$ ms). The triggered images were acquired in the late diastole where the pulsatile brain motion is negligible. Diffusion weighting was applied in left/right direction. The *b* values were (A, D) 2.7 s/mm^2, (B, E) 364 s/mm^2, and (C, F) 728 s/mm^2. Although no fat-suppression was used, the images do not show any off-resonance artifacts. All images are free of rigid-body motion artifacts. ECG gating improves the image quality due to a reduced background noise and fewer streaking artifacts. However, the images acquired without ECG gating show only some attenuation due to brain parenchyma pulsation in the central part of the brain.

gated acquisitions in slices with significant motion. In the *in vivo* studies, high-resolution DWI (in-plane resolution < 1 mm), anisotropy measurements, and investigations of the motion sensitivity were performed. A typical *in vivo* experiment consisted of the acquisition of five slices with two or more *b* values and diffusion weighting in all three orthogonal directions. The *b* values were stepped from 1.7 up to 728 s/mm^2. Without ECG-gating the total acquisition time was 4:16 min for a five-slice experiment with a 512 × 512 matrix and two *b* values, diffusion weighting in one direction, using a repetition time of $TR = 1$ s and $N = 4$ echoes per echo train. No special head restraint was used.

RESULTS

Phantom Studies

Diffusion measurements with diffusion weighting in all three orthogonal directions were performed on a water-filled phantom at room temperature (data not shown). Each ADC value was calculated from two optimally trimed images acquired at different *b* values. The nonlinear fit yielded the following diffusion coefficients: $ADC_x = (2.47 \pm 0.16) \cdot 10^3$ μm^2/s, $ADC_y = (2.37 \pm 0.14) \cdot 10^3$ μm^2/s and $ADC_z = (2.49 \pm 0.11) \cdot 10^3$ μm^2/s. The calculated average diffusion constant $ADC_{av} = (ADC_x + ADC_y + ADC_z)/3$ yielded a value of $ADC_{av} = (2.44 \pm 0.14) \cdot 10^3$ μm^2/s, which is in good agreement with the values of the diffusion constant for bulk water at room temperature reported in literature (*42*).

In Vivo Studies

Figure 6 compares ECG-gated versus ungated high-resolution DW-rTSE images using a 512 × 512 image matrix without self navigation. The triggered images were acquired in the late diastole where the pulsatile brain motion is negligible. In all images diffusion-weighting was applied in left/right direction with *b* values ranging from 2.7 to 728 s/mm^2. Although no fat suppression was used, the images do not show significant off-resonance artifacts, since a readout bandwidth of 100 kHz was used. Thus, fat causes only a shift of about one pixel in the radial direction. The rotation of the readout gradient smears out these small spatial shifts to a blurring of negligible amplitude in the final image. As depicted in Fig. 6, all images are nearly

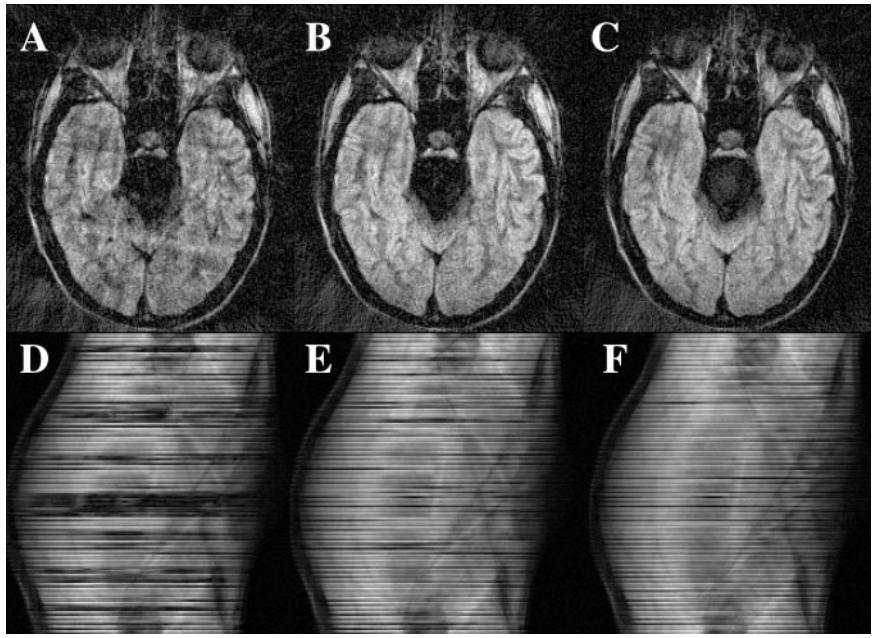

FIG. 7. Effect of self-navigator: Diffusion weighted images (A–C) with a *b* value of 692 s/mm^2 and the corresponding sinograms (D–F) are shown. Diffusion weighting was applied in slice direction. The repetition time was $TR = 5$ s. The artifacts due to pulsatile brain motion are strong if no ECG gating is used (A). They can be reduced when the degraded projections are acquired again using the self-navigation approach (B). Using ECG-gating completely eliminates artifacts (C). This can be observed in the corresponding sinograms (D–F) as well, where degraded projections appear as dark lines. This scenario represents the worst case, since a strong diffusion weighting in the main direction of motion was applied.

free of rigid-body motion artifacts. ECG gating reduces remaining weak streaking artifacts and background noise and improves the sharpness of the image. This is a clear sign that the main source of artifacts is pulsatile brain motion. Thus, the use of ECG gating provides a small increase in image quality but with the disadvantage of an significantly increased scan time: Scan time increases from 6:24 min without ECG gating (multislice mode 5 slices, 3 *b* values each, $TR = 1$ s) to approximately 32 min (single-slice mode, 5 single slices, 3 *b* values each, $TR = 1$ s) with ECG gating. The ECG-gated images were acquired in single-slice mode in order to provide reference images free of pulsatile brain motion artifacts from all slices. As can be seen, the images acquired without ECG gating show only some minor attenuation due to brain parenchyma pulsation in the central part of the brain. As a result, in most parts of the human brain neither ECG gating nor self-navigation are necessary (see also Figs. 8 and 9).

Figure 7 depicts the efficiency of the self-navigator approach in an inferior slice, which is known to be significantly affected by brain pulsation (*41*). Diffusion weighting was applied in head/foot direction, corresponding to main direction of brain motion. As seen in Fig. 7D, the projections which were acquired without ECG gating are degraded the most, resulting in a low image quality (Fig. 7A). In comparison, Fig. 7C shows that ECG gating provides the highest image quality, with the absence of corrupted projections in the sinogram (see Fig. 7F). Finally, Fig. 7B depicts the self-navigated image obtained without ECG gating, but where only $\frac{1}{4}$ of the motion corrupted projections were reacquired in a subsequent scan. The corresponding sinogram (Fig. 7E) shows a reduced amount of degraded projections, as compared to the ungated scan. This example demonstrates that ungated imaging in conjunction with self-navigation provides image quality almost comparable to fully ECG-gated acquisitions in areas of significant brain motion.

Figure 8 shows diffusion-weighted images and the corresponding ADC maps of different slices of the human brain. Diffusion weighting was applied in posterior/anterior direction, perpendicular to the main direction of pulsatile brain motion. The images are free of motion artifacts even though no ECG gating, no self-navigation, and no special head restraint was used. The images have an in-plane resolution of 700 μm and 8 mm through plane. Anatomical details such as the individual gyri and sulci can be identified clearly.

Figure 9 shows a slice through the ventricles of the human brain with diffusion weighting applied in all three orthogonal directions. Neither ECG gating nor self-navigation was used, since pulsatile brain motion can be neglected in this slice position. Diffusional anisotropy in white matter (WM) was observed in the regions of the corona radiata, where the ADC map shows higher values in case of diffusion weighting in slice direction (Fig. 9L) and lower values with diffusion weighting in-plane (Fig. 9D, H). Table 1 summarizes the measured ADC values in WM and GM. The variation of the ADC values for WM indicates the existence of fibers which run through the

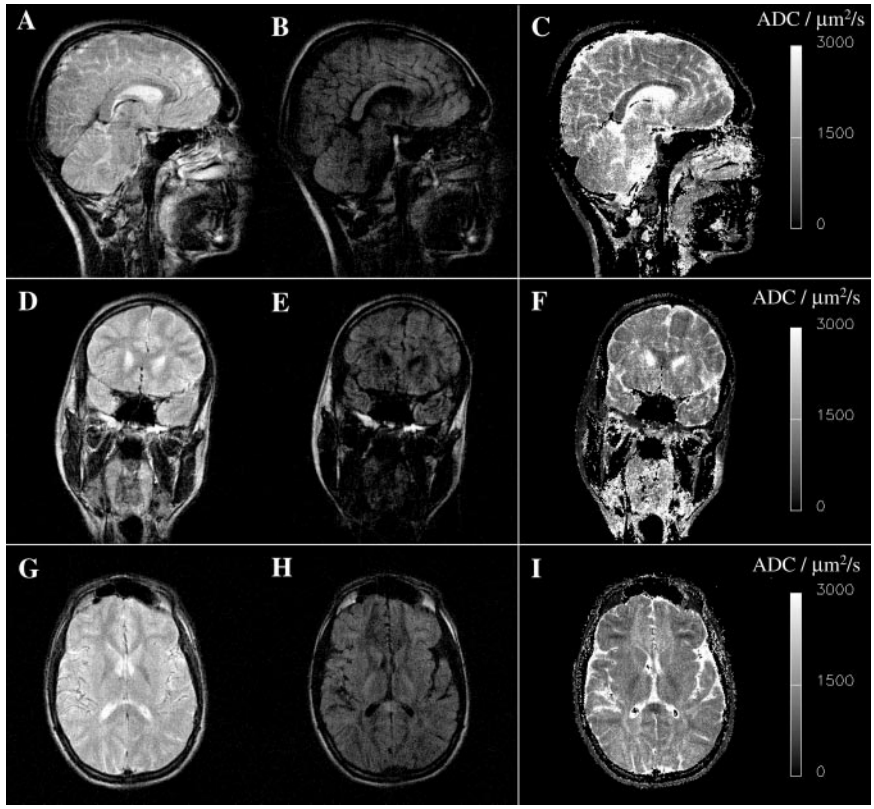

FIG. 8. High resolution DWI: This figure shows (A–C) sagittal, (D–F) coronal, and (G–I) transversal slices from the human brain with *b* values of (A, D, G) 2.7 s/mm^2 and (B, E, H) 728 s/mm^2 and the corresponding ADC maps (C, F, I). Diffusion weighting was applied in the posterior/anterior direction. No ECG gating nor special head restraint was used. The nominal resolution was 700 μm in-plane and 8 mm through-plane.

image plane. The measured ADC values are in the range of those previously published (*43–46*).

DISCUSSION

In this study, a modified radial turbo-spin-echo technique for high-resolution diffusion-weighted imaging and quantitative ADC mapping has been presented. The successful implementation of the DW-rTSE technique relied on an accurate analysis of eddy current and motion effects on diffusion weighted PR imaging. It was shown that a phase dispersion after the PGSE diffusion preparation is the common source of artifacts resulting from eddy currents and motion. Depending on the orientation of the diffusion weighting and the direction of the readout gradient, artifacts of different power are produced in the image. Based on this analysis, appropriate compensation techniques, an effective eddy current compensation, and a self-navigation approach were developed.

When compared with standard 2D-FT imaging, DW-rTSE produces images essentially free of rigid body motion artifacts with significantly reduced sensitivity to pulsatile brain motion. Images almost free of pulsatile motion artifacts were acquired without ECG gating or self-navigation from slices superior to the eyes. Images from slices inferior to the eyes showed an acceptable level of motion artifacts when acquired without ECG gating. Remaining artifacts were further reduced using the self-navigation approach. In contrast to single-shot DW techniques, DW-rTSE allows high-resolution DWI with an in-plane resolution of up to 700 μm on standard clinical scanners with imaging times significantly reduced compared to standard single-echo 2D-FT DWI. This “anatomical resolution” may allow detection of small lesions, definition of exact borders as well as accurate volumetric measurements.

To summarize, the modified DW-rTSE provides the following key properties:

- Diffusional anisotropy can be studied.
- Quantitative diffusion measurements are possible.
- Eddy current compensation eliminates artifacts due to eddy currents caused by the diffusion gradients.
- No cardiac gating is necessary for diffusion imaging in most regions of the human brain.
- Residual motion artifacts can be reduced by a self-navigation technique.

However, some critical issues remain. First, the proposed eddy current compensation scheme obviously performs only on systems where short-term (i.e., short relative to the inter echo

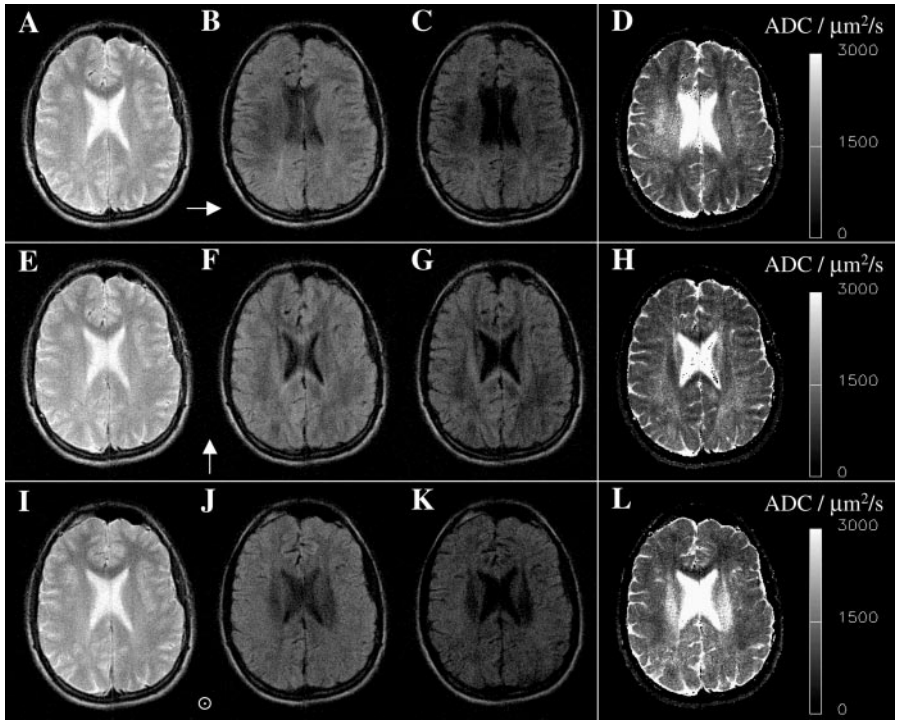

FIG. 9. Quantitative diffusion measurements: Diffusion-weighted images with weighting from (A–C) left to right, (E–G) posterior to anterior, and (I–K) head to foot and the corresponding ADC maps (D, H, L) are shown. The arrows symbolize the direction of diffusion weighting. Diffusional anisotropy is apparent in regions of the corona radiata where strong attenuation can be observed in the images with diffusion weighting in slice direction (K) in contrast to the hyper-intensity with weighting in posterior/anterior direction (G). ADC maps show the same effect, with a higher ADC value in this region with weighting in slice direction (L) and a much smaller ADC value with weighting in anterior/posterior direction (H).

spacings) eddy currents dominate. On imaging systems where long-term eddy currents are significant, additional trim gradients must be added before each individual readout. This was not necessary on our system, as clearly demonstrated in Fig. 5. In general, however, this eddy current compensation must be calibrated on a system-by-system basis.

The proposed self-navigation approach was developed for the particular case of significant brain motion. This is typically a problem in inferior slices when diffusion weighting is applied in head/foot direction. In this situation, the self-navigation approach comes at the expense of prolonged scan times, since approximately $\frac{1}{3}$ of the projections are corrupted by brain motion. However, in this case ECG gating, which would dictate the use of slow single-slice acquisitions, is completely avoided. Thus, multislice imaging can still be performed in clinically feasible experiment times as demonstrated by the *in vivo* results. Ideally, the reacquisition should be performed online for clinical efficacy, which was not yet possible with our system. In this ideal online situation the (i) acquisition of a complete set of projections would be directly followed by an (ii) automatic calculation of a threshold followed by (iii) a corresponding reacquisition of corrupted projections. Further work is required concerning the determination of the optimal number of echoes per readout period in order to obtain the highest image quality. The high-resolution achievable with the proposed method may increase the number of possible applications for DWI. For example it may allow the detection of small lesions caused by multiple sclerosis (*34, 35*) and offers the possibility to study the pathology of diseases that affect myelination. Clearly, clinical validation is required to test the performance of the self-navigator approach in patients and to evaluate lesion contrast-to-noise and border definition in stroke lesions.

In summary, the proposed DW-rTSE technique combines the resolution of conventional spin-echo 2D-FT imaging with

TABLE 1
ADC Values in Human Brain

$ADC/10^3\ \mu m^2\ s^{-1}$	Grey matter	White matter
ADC_x	0.9 ± 0.2	1.5 ± 0.3
ADC_y	1.0 ± 0.2	1.0 ± 0.2
ADC_z	1.0 ± 0.2	1.9 ± 0.4
ADC_{av}	1.0 ± 0.2	1.5 ± 0.3

Note. The ADC values were measured in an axial slice through the ventricles of human brain. The region of interest for white matter was located next to the ventricles in the corona radiata where anisotropy can be observed. Grey matter showed no anisotropy of diffusion.

the motion insensitivity of single-shot techniques. Since DW imaging has the potential to play an important role in the evaluation of patients with stroke and other diseases, the need for clinical widely available and robust sequences such as DW-rTSE will likely increase. Thus, further investigation concerning the application of radial DW sequences are promising.

ACKNOWLEDGMENT

Vladimir Jellus was supported by a grant of the Alexander-von-Humboldt-Stiftung.

REFERENCES

1. G. E. Wesbey, M. E. Moseley, and R. L. Ehman, Translational molecular self-diffusion in MRI measurements of the self-diffusion coefficient, *Invest. Radiol.* **19,** 491–498 (1984).
2. D. G. Taylor and M. C. Bushell, The spatial mapping of translational diffusion coefficients by the NMR imaging technique, *Phys. Med. Biol.* **30,** 345–349 (1985).
3. D. Le Bihan, E. Breton, D. Lallemand, P. Grenier, E. Cabanis, and M. Laval-Jeantet, MR imaging of intravoxel incoherent motions: Application to diffusion and perfusion in neurologic disorders, *Radiology* **161,** 401–407 (1986).
4. M. E. Mosley, Y. Cohen, J. Mintorovitch, and P. R. Weinstein, Early detection of regional cerebral ischemia in cats: Comparison of diffusion and T2-weighted MRI and spectroscopy, *Magn. Reson. Med.* **14,** 330–346 (1990).
5. M. E. Mosley, Y. Cohen, J. Mintorovitch, H. S. Asgari, M. F. Wendland, J. Tsuruda, and D. Norman, Diffusion-weighted MR imaging of anisotropic water diffusion in cat central nervous system, *Radiology* **176,** 439–445 (1990).
6. S. Warach, D. Chien, W. Li, M. Ronthal, and R. R. Edelmann, Fast magnetic resonance diffusion-weighted imaging of acute human stroke, *Neurology* **42,** 1717–1723 (1992).
7. D. Chien, K. K. Kwong, D. R. Gress, F. S. Buonanno, R. B. Buxton, and B. R. Rosen, MR diffusion imaging of cerebral infarction in humans, *Am. J. Neuroradiol.* **13,** 1097–1102 (1992).
8. A. C. Heide, T. L. Richards, E. C. Alvord Jr., J. Peterson, and L. M. Rose, Diffusion imaging of Experimental Allergic Encephalomyelitis, *Magn. Reson. Med.* **29,** 478–484 (1993).
9. E. O. Stejskal and J. E. Tanner, Spin diffusion measurements: Spin echoes in the presence of time-dependent field gradients, *J. Chem. Phys.* **42,** 288 (1965).
10. J. E. Tanner, Use of the stimulated echo in NMR diffusion studies. *J. Chem. Phys.* **42,** 2523–2526 (1970).
11. R. Turner and D. Le Bihan, Single shot diffusion imaging at 2.0 Tesla, *J. Magn. Reson.* **86,** 445–452 (1990).
12. R. Turner, D. Le Bihan, J. Maier, R. Vavrek, L. K. Hedges, and J. Pekar, Echoplanar imaging of intravoxel incoherent motions, *Radiology* **177,** 407–414 (1990).
13. S. Warach, J. Gaa, B. Siewert, P. Wielopolski, and R. R. Edelmann, Acute human stroke studied by whole brain echoplanar diffusion-weighted magnetic resonance imaging, *Ann. Neurol.* **37,** 231–241 (1995).
14. K. D. Merboldt, W. Haenicke, H. Bruhn, M. L. Gyngell, and J. Frahm, Diffusion imaging of the human brain *in vivo* using high speed STEAM MRI, *Magn. Res. Med.* **23,** 192–197 (1992).
15. M. Deimling, E. Mueller, and G. Laub, Diffusion weighted imaging with turbo-FLASH, *in* "Proc. SMRM 9th Annual Meeting," p. 387, Berkeley, CA (1990).
16. L. Guoying, P. Van Gelderen, J. Duyn, and C. T. W. Moonen, Single-shot diffusion MRI of human brain on a conventional clinical instrument, *Magn. Reson. Med.* **35,** 671–677 (1996).
17. K. D. Merboldt, W. Haenicke, M. L. Gyngell, J. Frahm, and H. Bruhn, Rapid NMR imaging of molecular self-diffusion using a modified CE-FAST sequence, *J. Magn. Reson.* **82,** 115–121 (1989).
18. K. D. Merboldt, W. Haenicke, M. L. Gyngell, J. Frahm, and H. Bruhn, The influence of flow and motion in MRI of diffusion using a modified CE-FAST sequence, *Magn. Reson. Med.* **12,** 198–208 (1989).
19. D. Le Bihan, Intravoxel incoherent motion imaging using steady-state free precession, *Magn. Reson. Med.* **7,** 346–351 (1988).
20. A. W. Anderson and J. C. Gore, Analysis and correction of motion artifacts in diffusion weighted imaging, *Magn. Reson. Med.* **32,** 379–387 (1994).
21. R. J. Ordidge, J. A. Helpern, Z. X. Qing, R. A. Knight, and V. Nagesh, Correction of motional artifacts in diffusion-weighted Mr images using navigator echoes, *Magn. Reson. Med.* **12,** 455–460 (1994).
22. A. De Crespigny, M. Marks, D. Enzmann, and M. Moseley, Navigated diffusion imaging of normal and ischemic human brain, *Magn. Reson. Med.* **33,** 720–728 (1995).
23. G. H. Glover and J. M. Pauley, Projection reconstruction techniques for reduction of motion effects in MRI, *Magn. Reson. Med.* **28,** 275–289 (1992).
24. K. J. Jung and Z. H. Cho, Reduction of motion artifacts in NMR diffusion imaging using view-angle tilted line-integral projection reconstruction, *Magn. Reson. Med.* **19,** 349 (1991).
25. P. T. Callaghan and C. D. Eccles, Sensitivity and resolution in NMR imaging, *J. Magn. Reson.* **71,** 426–445 (1987).
26. L. D. Hall and S. Sukumar, Rapid data-acquisition for NMR-imaging by the projection-reconstruction method, *J. Magn. Reson.* **56,** 179–182 (1984).
27. V. Rasche, D. Holz, and W. Schepper, Radial turbo spin echo imaging, *Magn. Reson. Med.* **32,** 629–638 (1994).
28. A. F. Gmitro and A. L. Alexander, Use of projection reconstruction method to decrease motion sensitivity in diffusion-weighted MRI, *Magn. Reson. Med.* **29,** 835–838 (1994).
29. T. P. Trouard, Y. Sabharwal, M. I. Altbach, and A. F. Gmitro, Analysis and comparison of motion-correction techniques in diffusion-weighted imaging, *J. Magn. Reson. Imaging* **6,** 925–935 (1996).
30. T. P. Trouard, R. J. Theilmann, M. I. Altbach, and A. F. Gmitro, Diffusion-weighted multislice projection reconstruction imaging on a clinical scanner, *in* "Proc. of the ISMRM, Vol. 3, 5th scientific meeting," Vancouver, B.C., Canada (1997).
31. T. P. Trouard, R. J. Theilmann, M. I. Altbach, and A. F. Gmitro, High-resolution diffusion imaging with DIFRAD-FSE (diffusion-weighted radial acquisition of data with fast spin-echo) MRI, *Magn. Reson. Med.* **42**(1), 11–18 (1999).
32. M. H. J. Seifert, C. Hillenbrand, V. Jellus, A. Haase, and P. M. Jakob, High resolution diffusion imaging using radial turbo-spin-echo sequence, *in* "Book of Abstracts, 16th Annual Meeting of ESMRMB," no. 460 (1999).
33. W. Dannels, Y. Xu, and H. Liu, Rotating diffusion MRI for reduced motion artifacts, *in* "Proc. of the ISMRM, Vol. 3, 5th Scientific Meeting," Vancouver, B.C., Canada (1997).
34. H. F. McFarland, The lesion in multiple sclerosis: Clinical, patho-

logical, and magnetic resonance imaging considerations, *J. Neurol. Neurosurg. Psychiatry* **64**(1), 26–30 (1998).

35. D. H. Miller, R. I. Grossman, S. C. Reingold, and H. F. McFarland, The role of magnetic resonance techniques in understanding and managing multiple sclerosis, *Brain* **121,** 3–24 (1998).

36. J. Hennig, Echoes—How to generate, recognize, use or avoid them in MR-imaging sequences, *Conc. Magn. Reson.* **3,** 125–192 (1991).

37. D. G. Norris, P. Börnert, T. Reese, and D. Leibfritz, On the application of ultrafast RARE experiments, *Magn. Reson. Med.* **27,** 142–164 (1992).

38. R. A. Brooks and G. di Chiro, Principles of computer assisted tomography (CAT) in radiography and radioisotopic imaging, *Phys. Med. Biol.* **21**(5), 714 (1976).

39. C. B. Ahn and Z. H. Cho, Analysis of eddy currents in magnetic resonance imaging, *Magn. Reson. Med.* **17,** 149–163 (1991).

40. A. L. Alexander, J. S. Tsuruda, and D. L. Parker, Elimination of eddy current artifacts in diffusion-weighted echo-planar images: The use of bipolar gradients, *Magn. Reson. Med.* **38,** 1016–1021 (1997).

41. R. Wirestam, D. Greitz, C. Thomsen, S. Brockstedt, M. B. E. Elsson, and F. Ståhlberg, Theoretical and experimental evaluation of phase-dispersion effects caused by brain motion in diffusion and perfusion MR imaging, *J. Magn. Reson. Imaging* **6,** 348–355 (1996).

42. R. Mills, Self-diffusion in normal and heavy water in the range 1–45°, *J. Phys. Chem.* **77**(5), 685–688 (1973).

43. D. Le Bihan (Ed.), "Diffusion and Perfusion Magnetic Resonance Imaging: Applications to Functional MRI," Raven Press, New York (1995).

44. Perman, Gado, and Sandstrom, DPSF: Snapshot FLASH diffusion/perfusion imaging, *in* "Proc. of the 9th Annual Meeting of the SMRM," p. 387, Berkeley (1990).

45. D. Chien, R. Buxton, K. K. Kwong, T. J. Brady, and B. R. Rosen, Quantitative diffusion imaging in the human brain, *in* "Proc. of the 7th Annual Meeting of the SMRM," p. 218, San Francisco (1988).

46. J. C. Falconer and P. A. Naryana, Cerebrospinal fluid-suppressed high resolution diffusion imaging of the human brain, *Magn. Reson. Med.* **37,** 119–123 (1997).

47. V. Rasche, "Möglichkeiten schneller Bildgebung mittels radialer Akquisitionsschemata in der Kernspintomographie," Ph.D. thesis, Physics Department, University of Bielefeld (1995).